

# AN IMAGE FILTER TECHNIQUE TO RELAX PARTICLE IMAGE VELOCIMETRY

L. Rockstroh, S. Wahl, Z. Wang, P. Werner, S. Simon

University Stuttgart, Institute of Parallel and Distributed Systems, Germany

## ABSTRACT

*The method particle image velocimetry (PIV) measures particle velocities in natural sciences and engineering based on the determination of the optical flow. Classical PIV requires capturing the particles twice with short delay and with very short exposure time which exceeds the frame rate and the shutter speed of typical imaging systems. Thus, the exposure time is realized with illumination bursts based on double pulse lasers and imaging systems capable of high frame rates are used for capturing the particles. In order to relax PIV measurements, a filter technique is presented that generates both snapshots out of only one single image. This image is captured with a standard imaging system with standard exposure times which relaxes the constraints of the PIV measurement setup significantly. The filter technique is based on spatial filters and its computational complexity is independent from the image content. It also enables the integration of the technique into embedded architectures for real-time PIV. The functionality is demonstrated by taking the example of a particle-based manufacturing process and the measuring error caused by the filter technique is analyzed.*

**Index Terms**— Particle image velocimetry, Image motion analysis, Segmentation, Filtering algorithms.

## 1. INTRODUCTION

Classical particle image velocimetry (PIV) is a technique to measure particle velocities based on two snapshots of the particles which are taken at times  $t$  and  $t + \delta t$  [1]. Both snapshots contain dot-like projections of mostly the same particles but with spatial displacements due to the particle velocities and  $\delta t$ . In order to determine those displacements for different areas of the snapshots, both of them are divided into multiple interrogation windows of equal size. Afterwards, each window of the first snapshot is cross-correlated with its counterpart of the second snapshot. Here, a cross-correlation equals a search for a pattern match of a particle constellation and the result represents the spatial displacement of the particle projections contained in this constellation.

PIV provides a motion vector for each pair of interrogation windows which is why the accuracy of PIV depends on constant particle velocities inside those windows. Also, the size of the interrogation windows must cover the spatial offset of the particles in order to detect the displacement.

Another constraint for PIV measurements is the absence of motion blurring so that the PIV algorithm detects the distance between the projections of the same particle rather than the distance between the motion blurring of different particles. Such dot-like projections require even for low particle velocities short exposure times in the

nanosecond range that exceed the shutter speed of typical imaging systems [2]. Exposure times in that range can be achieved by using pulsed light sources, such as lasers, so that the effective exposure time is determined by the pulse length of the light source instead of the shutter of the imaging system.

In this paper, an image filter technique with linear processing time is proposed that relaxes PIV by enabling measurements based on single images. These images are captured with exposure times that are achievable with typical imaging systems, and thus, each of them contains the motion blurring of many particles. Based on the start and end of each motion blurring, the two different particle positions required for PIV are extracted and the PIV results are divided by the exposure time in order to calculate the particle velocities.

In contrast to many established methods capable of detecting the starts and ends of those motion blurring, the processing time of the filter technique which is proposed here, does not depend on the content of the image. This favors the integration of the technique into embedded architectures for real-time PIV measurements that have been reported in the past [3, 4].

The remainder of this paper is organized as follows. Established methods to detect lines and line endings are discussed in Section 2. An alternative filter technique is proposed in Section 3 and an error analysis of this technique is made in Section 4. Section 5 shows experimental results and finally, Section 6 concludes this paper.

## 2. STATE OF THE ART

In this section, established methods for detecting lines and line endings are discussed. One of those methods is the Hough transform which determines the location of straight lines or other geometrical shapes [5]. This transform has an expensive but linear processing time which is independent from the image content and successful attempts to optimize the processing time have been made [6]. However, the method does not detect the start and end of a line which requires a post-processing stage.

Another drawback inherent to the Hough transform is its inability to distinguish between a short continuous line and a set of distinct points that are arranged in a line for any reason. As a consequence, horizontally aligned lines, which are arranged side by side, will erroneously trigger the detection of vertical lines that contain one pixel from each of the original horizontal lines. However, typical particle observations contain huge quantities of parallel, motion blurring and thus, applying Hough transform on these images results in many erroneous detected lines.

Other established methods to detect the endpoints of thin lines in linear time are the hit-or-miss transformation (HMT) [7] and the rotating kernel transformation (RKT) [8]. However, the width of the motion blurring to be processed is several pixels in size. It

depends on the brightness of the particle and of the background as well as on the modulation transfer function which varies with the distance of the particle from the focal plane [9].

The transformation from motion blurring with arbitrary width into thin lines that are processible by HMT or RKT can be accomplished by using ridge detection. Ridge detection is mainly based on watershed- [10], region growing- [11], morphological [12] or multi-scale- [13] approaches which all have in common that their processing times depend on the content of the image. However the processing time of the filter technique presented in this paper is independent from the amount, width or length of the occurring motion blurring.

### 3. FILTER TECHNIQUE TO RELAXATION OF PARTICLE IMAGE VELOCIMETRY

The relaxation of PIV presented here is based on a simplification of its measurement setup. Instead of capturing sharp projections of the same particles twice, the motion blurring of those particles is captured only once which is easier to accomplish [2]. Afterwards, linear spatial filters are applied on the captured image in order to extract the starts and ends of the motion blurring. Finally, the detected start and end positions are separated into two images which are the input to the PIV algorithm.

This Section is structured as follows: The first Subsection describes the filtering of motion blurring with angles between -45 and +45 degree to the horizontal which is sufficient for many thermal spraying applications. Based on Subsection 1, Subsection 2 discusses filtering motion blurring with arbitrary angle.

#### 3.1 Filtering of Motion Blurring with Angles of up to 45 Degree

The filtering of motion blurring with angles between -45 and +45 degree is sufficient for many thermal spraying applications where the occurring angles of motion blurring are in that range [4]. In order to detect the start and end positions of those blurring, two spatial filters are applied separately on the input image.

$$S_x^+ = \begin{bmatrix} 1 & 2 & -i & -2 & -1 \\ 4 & 8 & -i & -8 & -4 \\ 6 & 12 & 0 & -12 & -6 \\ 4 & 8 & -i & -8 & -4 \\ 1 & 2 & -i & -2 & -1 \end{bmatrix} \quad S_x^- = \begin{bmatrix} -1 & -2 & -i & 2 & 1 \\ -4 & -8 & -i & 8 & 4 \\ -6 & -12 & 0 & 12 & 6 \\ -4 & -8 & -i & 8 & 4 \\ -1 & -2 & -i & 2 & 1 \end{bmatrix} \quad (1)$$

Formula 1 shows the kernels of the spatial filters  $S_x^+$  and  $S_x^-$  which consist of the vertical Sobel operator that is supplemented by a parameter "i". This parameter causes the partial suppression of the vertical component of particle trajectories that are not completely horizontal. The effect is shown in Fig. 1 for motion blurring with different angles, where  $S_x^-$  filters the start and  $S_x^+$  the end of the motion blurring. Here, in contrast to the Sobel results, which are only useful for horizontal blurring, the  $S_x$  results also contain the separated start and end of the blurring with a 45 degree angle. The suppression factor "i" is a parameter for the sensitivity of the filter. Its optimal setting depends on the following three parameters:

1. **Maximum occurring angle**  
The intensity of the response of the vertical Sobel component increases with the angle of the motion blurring. Thus, high angles require a high suppression factor.
2. **Modulation transfer function (MTF)**  
The MTF describes the loss of contrast that occurs when capturing an object onto an image. The loss depends on the quality and properties of the components of the imaging system and progresses with increasing distance of the object from the focal plane. The consequence of this loss of contrast is a reduced intensity of the Sobel filter response on edges and ridges. Hence, low contrast conditions require a low suppression factor so that the Sobel response at the start and end of the motion blurring is maintained. Another effect is that, when captured with low magnification, the size of the projections of small particles depends mainly on the MTF rather than on the size of the particles.
3. **Brightness of particles and background**  
The difference between the brightness of a particle and the brightness of the background impacts on the signal strength of the captured particle. This signal strength influences the contrast which has an effect on the Sobel filter results. Additionally, the values of both brightnesses determine the effectiveness of the suppression factor.  
Besides the impacts of illumination and physical properties of the particles, the brightnesses depend on various settings of the imaging system like dynamic range enhancements, signal amplification, bias and others. Another influence on the brightness of the particles is the MTF. Here, the smoothening effect of the MTF decreases the intensity of small projections and thus, the effectiveness of the suppression factor is reduced.

Besides the variety of influences discussed above, the filter technique must suppress the vertical component of motion blurring in any occurring scenario while providing as many start and end positions as possible. Thus, the smallest possible suppression factor is chosen based on the worst case scenario. Here, the worst case includes the highest contrast, which occurs for objects on the focal plane, the highest angle and the highest particle brightness that may occur. Then, in any other scenarios the filter will also suppress vertical components of motion blurring because those scenarios will derive from the worst case conditions.

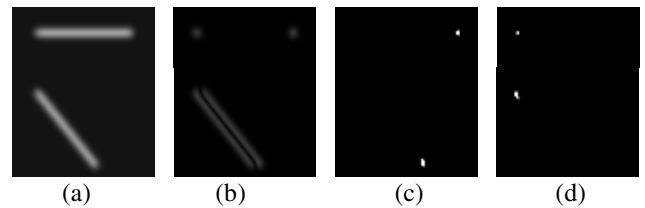


**Fig. 1.** Motion blurring with 0 and 45 degree angle (a), vertical Sobel results (b),  $S_x^+$  results (c) and  $S_x^-$  results (d).

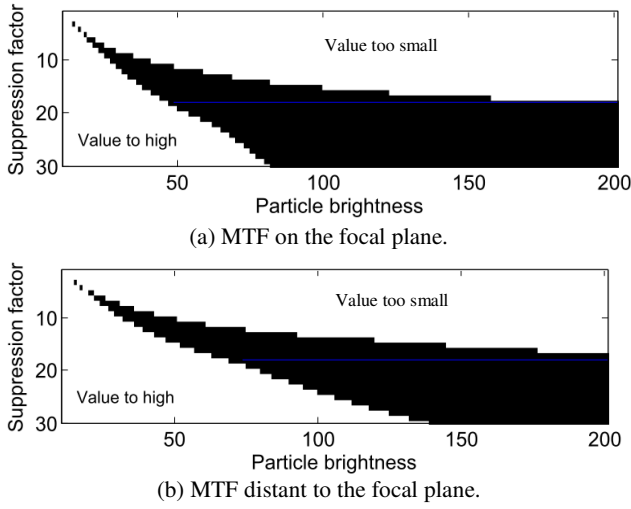


**Fig 2.** Suppression factor in dependence of the particle brightness for different MTF.

Determining the suppression factor requires specifying some of the parameters discussed above such as average background brightness, maximum occurring angle and the MTF on the focal plane. Fig. 2a shows the range of useful suppression factors (black) in dependence of the particle brightness and for a MTF that is related to the focal plane. The figure is based on motion blurring with an angle 45 degree, the brightness of the background was set to 10 and the effect of the MTF was approximated with a Gauss filter. The area in the bottom left corner represents values where the filter suppresses any responses of its Sobel component including the start and end positions of the motion blurring. Accordingly, the area on the top represents values where the filter fails to suppress the vertical component of the motion blurring. Thus, in example of Fig. 2a, 18 is the lowest acceptable suppression factor for a particle brightness of 200 which also works for particle brightnesses down to 50.

Fig. 2b is based on the same constrains as Fig. 2a except for a MTF that applies for objects with some distance to the focal plane. As a consequence the contrast is reduced and the Sobel response is less intense which requires a lower suppression factor. However, a suppression factor of 18, which was determined based on Fig. 2a, enables correct filtering for particle brightnesses in the range from 75 to 200.

### 3.2 Filtering of Motion Blurring with Arbitrary Angle

The filter technique discussed in Section 3.1 is based on the spatial filters  $S_x^+$  and  $S_x^-$  that consist of a vertical Sobel filter and a suppression factor that counteracts the Sobel response on the vertical component of angled motion blurring. However, for particle trajectories with angles larger than 45 degree, the suppression factor cannot compensate for the increasing intensity of the vertical Sobel component. Hence,  $S_x^+$  and  $S_x^-$  respond to the vertical component similar to the vertical Sobel such as shown in Fig. 3. In those cases, PIV measures the distance between the two lines which corresponds to the width of the motion blurring rather than to its length. However,  $S_y^+$  and  $S_y^-$  (Formula 2), which are 90 degree rotations of  $S_x^+$  and  $S_x^-$ , will obviously filter the start and end of motion blurring with angles between 45 and 135 degree.



**Fig. 3.** Particle trajectory with 70 degree angle (left) and filter results for  $S_x^+$  and  $S_x^-$  overlaid in one image (right).

$$S_y^+ = \begin{bmatrix} -1 & -4 & -6 & -4 & -1 \\ -2 & -8 & -12 & -8 & -2 \\ -i & -i & 0 & -i & -i \\ 2 & 8 & 12 & 8 & 2 \\ 1 & 4 & 6 & 4 & 1 \end{bmatrix} \quad S_y^- = \begin{bmatrix} 1 & 4 & 6 & 4 & 1 \\ 2 & 8 & 12 & 8 & 2 \\ -i & -i & 0 & -i & -i \\ -2 & -8 & -12 & -8 & -2 \\ -1 & -4 & -6 & -4 & -1 \end{bmatrix} \quad (2)$$

In order to detect the length of motion blurring for particle trajectories with arbitrary angle, the input images are processed by the algorithm presented in Listing 1. The input image is convolved with  $S_x^+$ ,  $S_x^-$ ,  $S_y^+$  and  $S_y^-$  (Line 1-4). Afterwards, PIV is executed twice for each pair of interrogation windows, once for the results of  $S_x^+$  and  $S_x^-$  and once for the results of  $S_y^+$  and  $S_y^-$  (Line 8-9). At least one of those two calculations will output the length of the motion blurring while the other one might respond to the width of the motion blurring. Due to the fact that the value of the width of a particles motion blurring is smaller than the value of its length, the PIV result with the larger value is selected (Line 10-13). This choice is based on the assumption that all particles inside an interrogation window have similar trajectories. However, similar particle trajectories in local areas of the size of the interrogation windows are already a constraint for correct PIV results (see Section 1).

**Listing 1.** Pseudo code of the filtering technique.

```

1 F1 = ( input_image * S_x^+ )
2 F2 = ( input_image * S_x^- )
3 F3 = ( input_image * S_y^+ )
4 F4 = ( input_image * S_y^- )
5
6 For i1 = 1: #(int_windows_x)
7   For i2 = 1: #(int_windows_y)
8     R1( i1, i2 ) = PIV( F1( i1, i2 ), F2( i1, i2 ) )
9     R2( i1, i2 ) = PIV( F3( i1, i2 ), F4( i1, i2 ) )
10    If |R1( i1, i2 )| > |R2( i1, i2 )| then
11      R3( i1, i2 ) = R1( i1, i2 )
12    Else
13      R3( i1, i2 ) = R2( i1, i2 )
14    End for
15  End for
16 Return R3

```

The pseudo code shown in Listing 1 provides results for arbitrary particle trajectories in terms of angle and value but cannot extract the sign of the trajectories. Determining those requires initial clues by the user based on which the sign for each pair of interrogation windows is extrapolated by applying a breadth first search.

#### 4. ERROR ANALYSIS

The impact of the filter technique on the accuracy of PIV was determined by comparing classical PIV to PIV with filtered motion blurring for single particle trajectories. The comparison is based on the tool PIVlab, which calculates the displacements of particle projections in x- and in y-direction [14].

Table 1 shows offsets of those displacements, which are caused by the filters  $S_x^+$  and  $S_x^-$ , for different diameters of particle projections and for various angles of particle trajectories. The offsets in x-direction depend on the diameter of the particle projections which is mostly attributed to the fact that the length of the motion blurring is not equivalent to the length of the particle trajectory. Instead, as illustrated in Figure 4, the motion blurring of a particles trajectory is around one particle projections diameter longer than the particle trajectory itself. In order to counteract this effect, the particle projections diameter can be subtracted from the measured displacement in x-direction.

**Table 1.** Offsets of PIV results caused by the filters  $S_x^+$  and  $S_x^-$ , in pixels.

Angle in degree	Offset in pixels for different diameters ( $\varnothing$ )					
	$\varnothing$ 5 pixel		$\varnothing$ 7 pixel		$\varnothing$ 9 pixel	
	x-direction	y-direction	x-direction	y-direction	x-direction	y-direction
0	5.7	-0.0	7.9	-0.0	10.0	-0.0
5	5.7	-0.1	8.1	-0.1	9.9	-0.0
10	5.6	-0.3	8.3	-0.2	10.0	-0.2
15	5.6	-0.4	8.3	-0.3	10.0	-0.3
20	5.6	-0.4	8.3	-0.3	9.9	-0.4
25	5.7	-0.6	8.3	-0.3	10.0	-0.6
30	5.6	-1.0	8.3	-0.5	10.1	-0.6
35	5.6	-0.9	8.2	-0.6	10.2	-0.7
40	5.6	-1.0	8.2	-0.6	10.1	-1.0
45	5.6	-1.4	8.2	-0.8	10.1	-1.0
50	5.6	-1.8	8.1	-1.0	10.0	-1.8
55	5.5	-2.8	8.0	-1.6	9.8	-2.3

Concerning the offset in y-direction, Table 1 shows negative values that depend on the angle of the particle trajectory. The reason for this dependency is that with increasing angle, the vertical component of the trajectory causes the filter results to extend in y-direction and as a consequence, the distance in y-direction is reduced. The effect can be seen in Figure 1c and 1d when comparing the filter results of the horizontal trajectory to those of the angled ones.

Figure 4 shows offsets of the total length of measured particle trajectories, once filtered with  $S_x^+$  and  $S_x^-$  and once filtered with  $S_y^+$  and  $S_y^-$ . The offset calculations are based on particle trajectories with a length of 50 pixels and the results have been corrected by the diameter of the particle projection.

PIV based on  $S_x$  filters (dashed line) measures a length of around 50 pixels (offset of 0 pixels) for angles between 0 and 58 degree

and a length of around 5 pixels (offset of -45 pixels) for angles between 59 and 90 degree. The reason for the loss in accuracy is the impact of the vertical component of angled particle trajectories. This phenomenon was discussed in Section 2 (see Fig. 2) and affects the PIV results based on  $S_y$  filters (dotted line) for angles between 0 and 31 degree in the same way.

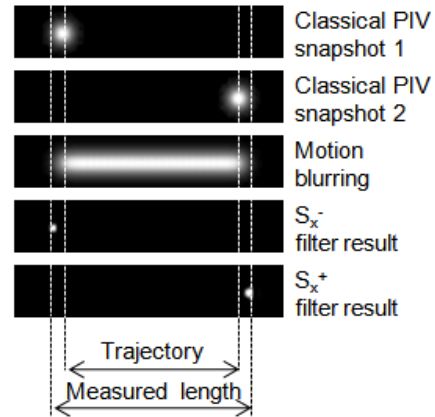


**Fig. 4.** Actual length and measured length of a particle trajectory based on filtered motion blurring.

According to the algorithm of Listing 1, PIV results are calculated based on the  $S_x$  filters as well as based on the  $S_y$  filters and the maximum of both calculations is selected as measurement result. Thus, the maximum offset for angles between 0 and 90 degree shown in Fig. 5 is 0.7 pixels and the lowest offset is -0.5 pixels. The offsets for angles between 90 and 360 degree are limited to the same values due to reasons of symmetry.

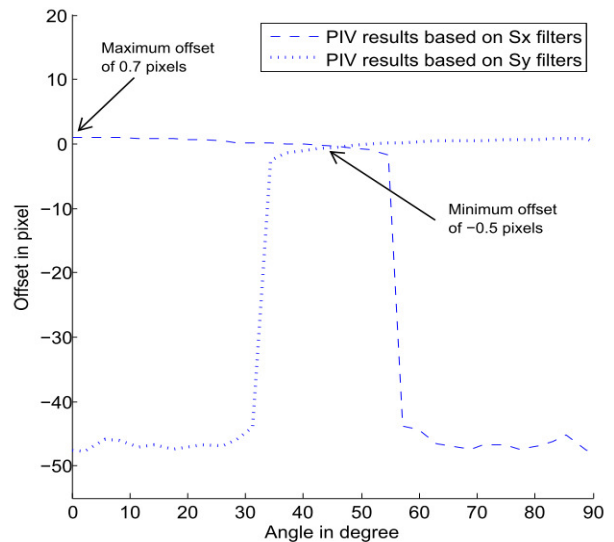


**Fig. 5.** Offset of the length of particle trajectories due to the filter technique for particle projections with a diameter of 5 pixels and a length of 50 pixels.

For motion blurring with a length of 30 pixels or longer, which is common for thermal spraying observations, an offset of 0.7 pixels equals a maximum relative error of 2.3 percent. A further improvement of the accuracy in general could be achieved by introducing a correction factor for the measured angle of the particle trajectories.

## 5. EXPERIMENTAL RESULTS

The filter technique was evaluated by using the example of thermal spraying processes which are based on high velocity particle flows. These particle flows have a preferred direction of flight and form spray plumes with conical shape.

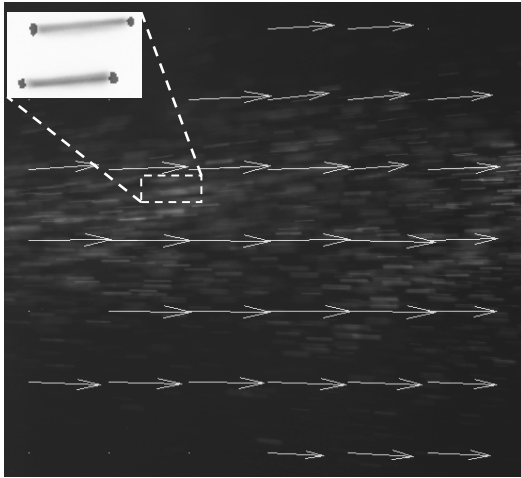


**Fig. 6.** PIV results of a thermal spraying observation based on filtered motion blurring.

Images that contain the motion blurring of thermal spraying particles have been filtered and the filter results were used for PIV calculations with PIVlab. The detail enlargement of Figure 6 shows the motion blurring of some thermal spraying particles as well as the filter results of  $S_x^+$  and  $S_x^-$  overlaid into the image. The large picture of Figure 6 shows an image from a thermal spraying observation, where the direction of flight is from left to right, overlaid with the results of PIVlab. These results confirm the conical shape of the spray plume and reveal the fact that particles in the outer regions of the spray plume are slower than in the center.

## 6. CONCLUSION

The filter technique presented in this paper relaxes particle image velocimetry (PIV) measurements by reducing the number of required snapshots from two to one. The functionality of this technique was proven for various diameters of the particle projections by taking the example of thermal spraying processes and the error induced by this modification was evaluated. Techniques for minimizing the measurement error have been discussed and one of them was applied to the measuring results. For particle projections of 5 pixels in diameter, the presented filter technique adds a value between -0.5 and 0.7 pixels to the determined length of particle trajectories when compared to

classical PIV without filtering. This results in a maximum relative error of 2.3 percent for typical thermal spraying measurements, which is acceptable for typical applications.

## 7. ACKNOWLEDGEMENTS

We like to thank Prof. R. Gadow from the Institute for Manufacturing Technologies of Ceramic Components and Composites in Stuttgart for providing us with images of thermal spraying processes.

## REFERENCES

- [1] C. Gray, et al., "High-speed PIV using high-frequency diode-pumped solid state laser and multi-frame CCD," Instrumentation in Aerospace Simulation Facilities, 19th International Congress on ICIAAF 2001, Cleveland, pp.135-139, 2001.
- [2] L. Rockstroh, J. Hillebrand, M. Shaikh, S. Röck, A. Killinger, A. Verl, S. Simon, and R. Gadow, "A particle image velocimetry method for low illumination conditions in thermal spray processes," in Proceedings of International Thermal Spray Conference 2010 (ITSC), Singapore, 2010.
- [3] A. Aubert; N. Bochar; V. Fresse, "An adaptive embedded architecture for real-time particle image velocimetry algorithms." In Proceedings of 14th European Signal Processing Conference (EUSIPCO), 2006, Florence.
- [4] H. Yu, M. Leeser, G. Tadmor, S. Siegel, "Real-Time Particle Image Velocimetry for Feedback Loops Using FPGA Implementation." In Proceedings of 43rd AIAA Aerospace Sciences Meeting and Exhibit, Reno, Nevada, 2005.
- [5] R. O. Duda, P. E. Hart, "Use of the Hough Transformation to Detect Lines and Curves in Pictures," Communications ACM, Vol. 15, No. 1, pp. 11-15, 1972.
- [6] H. Li, M.A. Lavin, R.J. Le Master, "Fast Hough Transform: A Hierarchical Approach", Computer Vision, Graphics, and Image Processing 36, pp. 139-161, 1986.
- [7] R.C. Gonzalez, R.E. Woods, Digital Image Processing, Prentice Hall, New Jersey, 2001.
- [8] Y.K. Lee, W.T. Rhodes, "Nonlinear image processing by a rotating kernel transformation", Optics Letters, Vol. 15, No. 23, pp. 1383-1385, 1990.
- [9] G. D. Boreman, "Modulation Transfer Function in Optical and Electro-Optical Systems", SPIE Press, Bellingham, 2001.
- [10] A.M. Lopez, F. Lumberras, J. Serrat, J.J. Villanueva, "Evaluation of methods for ridge and valley detection", Pattern Analysis and Machine Intelligence, Vol. 21, no. 4, pp 327-335, 1999.
- [11] S. Gautama, W. Goeman, J. D'Haeyer: "Robust detection of road junctions in VHR images using an improved ridge detector", Proceedings of ISPRS Congress, Istanbul, 2004.
- [12] J.A. Noble, "Morphological Feature Detection", Second International Conference on Computer Vision, Tampa, Florida, 1988.
- [13] T. Lindeberg, "Edge Detection and Ridge Detection with Automatic Scale Selection", International Journal of Computer Vision, Vol. 30, No. 2, 1998.
- [14] W. Thielicke and E.J. Stamhuis: PIVlab – time-resolved digital particle image velocimetry tool for matlab. <http://PIVlab.blogspot.com>, 2010.